B-Scan in a Reverberation Chamber

Qian Xu, Yi Huang, *Senior Member, IEEE*, Lei Xing, Zhihao Tian, *Student Member, IEEE*, Manoj Stanley and Sheng Yuan

***Abstract*—In this paper, the B-scan technique is applied to a reverberation chamber (RC) for the first time to characterize the time domain behavior of the chamber. Based on B-scan measurement results, three things are studied in this paper: 1) the statistical behavior of the fields in the time domain is investigated, and it is found that the received power of the impulse response follows chi-square distribution with one degree of freedom; 2) the stirrer efficiency is quantified based on the equivalent total scattering cross section (TSCS) of stirrers, and this definition is not sensitive to the antenna position and load in the RC. It is shown that the stirrer efficiency defined in this paper provides, for the first time, a quantitative way to evaluate the stirrer design and the chamber performance; 3) A time-gating technique is proposed which provides an alternative method to eliminate the early time response and obtain the chamber transfer function of the RC accurately. This could be potentially used to increase the stirrer efficiency without changing the stirrers physically. It is demonstrated that the B-scan technique is a very useful approach for the study and evaluation of an RC.**

***Index Terms*—B-scan, reverberation chamber, scattering cross section, stirrer efficiency, time domain technique.**

I. Introduction

THE time domain behavior of reverberation chambers (RC) has been studied in [1-6] to characterize the field inside RC. Information extracted from the time domain can be combined with that from the frequency domain, and a series of applications become possible, such as measuring the radiation efficiency of antennas without using a reference antenna [7], absorption cross section measurement [8], *Q* factor extraction and chamber decay time control [9]. A B-scan is a two-dimensional time domain impulse scan and has been widely used in many applications such as radar, medical imaging, non-destructive testing [10]. Some relevant work has been reported in [1, 2], which provide important insight of the chamber from the time domain, and the synthetic-aperture technique was used with 9 stirrer positions [1, 2]. In the time domain, the arrived signal at different times and from different angles can be observed directly providing important guidelines and insights for future measurements. However, a complete B-scan has not yet been obtained in an RC.

In this paper, a B-scan technique is applied to an RC which provides an alternative method to understand and characterize the time domain behavior of an RC. The statistical behavior of RCs in the frequency domain has been well investigated [11, 12], and the statistical distributions of the electric field in the frequency domain are well-known. However, there are limited studies on the time domain statistical distribution, which is one of the main contributions of this paper.

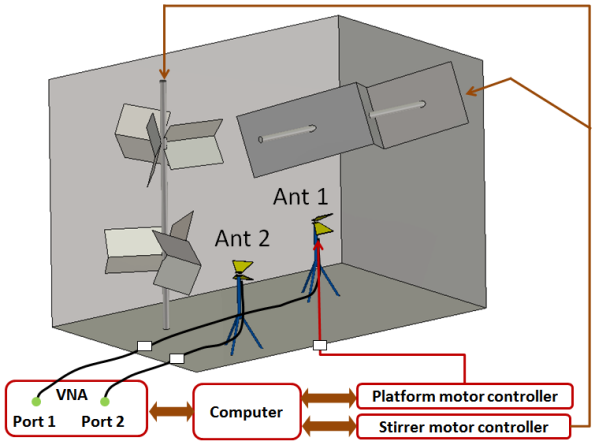

(a)

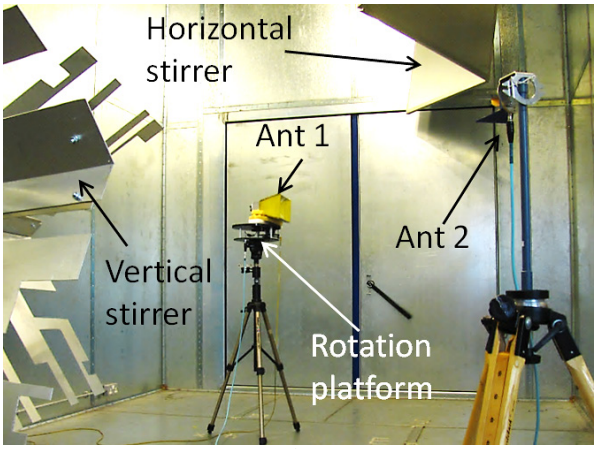

(b)

Fig. 1. B-scan measurement setup in an RC: (a) schematic measurement setup, (b) measurement setup in the RC at the University of Liverpool.

The stirrer efficiency is a very important parameter but hard to quantify in the frequency domain. Currently there is no standard definition of the stirrer efficiency. Many efforts have been made to discuss it [13-24], which have provided important practical guidelines and experience. It has been found that, the

Manuscript received Oct. 1, 2015. Corresponding author: Y. Huang.

Q. Xu, Y. Huang, Z. Tian, M. Stanley and S. Yuan are with the Department of Electrical Engineering and Electronics, The University of Liverpool, Liverpool, L69 3GJ, UK (e-mail: qian.xu@liv.ac.uk; yi.huang@liv.ac.uk; zhihao.tian@liv.ac.uk; manoj.stanley@liv.ac.uk; sgsyuan@liv.ac.uk).

L. Xing is with College of Electronic and Information Engineering, Nanjing University of Aeronautics and Astronautics, 211106, China. (e-mail: xinglei@nuaa.edu.cn)

stirrer efficiency (if defined using *K*-factor or independent sample numbers) could be changed by a load or different antenna positions. Thus, it is related to too many variables and hard to characterize in the frequency domain. Efforts have also been made in the time domain to characterize the stirrer efficiency based on the time domain cross-correlation [25], but the results are still sensitive to the load and loss in the RC. In this paper, a new definition of stirrer efficiency is proposed in the time domain and it is only related to the equivalent *total scattering cross section* (TSCS) of the stirrers and the volume of the RC. The equivalent TSCS of stirrers is determined by the geometric properties of the stirrers (size, shape, position, *etc*.) and how the stirrers are moved; it is not sensitive to the load and antenna position because the loss is corrected as can be seen later in (12). Like the definition of efficiency in other applications (radiation efficiency, converting efficiency, etc.), the stirrer efficiency defined in this paper is a quantifiable parameter in the range of 0% to 100% which correspond to an RC with no stirrer and to a perfect stirrer respectively. The definition in this paper provides a universal and quantitative way to compare the performance between different RCs or different stirrer designs in an RC which should be extremely useful for RC design.

Moreover, a time-gating technique has been used to remove the early-time behavior in the chamber decay constant extraction [7, 26], it is found in this paper that the time-gating technique can also be used in an RC to filter the unwanted signals to obtain the chamber transfer function accurately.

This paper is organized as follows: the measurement setup and theory are given first in Section II, followed by the understanding and discussion of the results in Section III where three aspects are addressed: the statistical behavior, stirrer efficiency quantification and time-gating technique. Finally, discussions and conclusions are summarized in Section IV.

II. B-Scan Measurement And Theory

To realize a B-scan in an RC, it is possible to measure the time domain response directly using an impulse source and an oscilloscope [27]. Another method is to measure the system response in the frequency domain and then apply the inverse fast Fourier transform (IFFT) to obtain the time domain response. Measuring the frequency domain response using a vector network analyzer (VNA) is simpler and can provide a larger dynamic range than a measurement directly in the time domain using an oscilloscope [28]. In this paper, the frequency domain measurement method is used to obtain the time domain response.

The measurement setup is shown in Fig. 1, the size of the RC is 3.6 m (*W*) × 5.8 m (*L*) × 4 m (*H*). Two horn antennas are used as antenna 1 (Rohde & Schwarz® HF 906) and antenna 2 (SATIMO® SH 2000). The rotation platform, stirrers and VNA are synchronized and controlled by a computer. *S*-parameters with 10001 sample points in the frequency range of 2 GHz to 4 GHz are recorded for different antenna angles and stirrer positions. For each antenna angle, 100 stirrer positions are used with 3.5 degrees/step. Antenna 1 is rotated with 2 degrees/step for one complete revolution. Thus there are 180 × 100 = 18000 sets of *S*-parameters in total.

The time domain response can be obtained from the IFFT of the measured *S*-parameters, and a 10th order elliptic band-pass filter is applied to reduce the ripples caused by a rectangular window [29], of which the pass band is set to be 2.4 GHz ~ 3.6 GHz. We denote the electric field at the receiving antenna as

$$E(t,\theta,n) = IFFT\left[\tilde{S}(\theta,f,n)\right], \tag{1}$$

where $\tilde{S}$ represents the filtered *S*-parameters depends on the rotation angle of antenna 1 (θ), frequency (f) and stirrer position (n). The plots of $IFFT\left[\tilde{S}_{11}(\theta,f,n)\right]$ and $IFFT\left[\tilde{S}_{21}(\theta,f,n)\right]$ give monostatic and bistatic B-scan maps respectively. It should be pointed out that the electric field obtained from the IFFT of *S*-parameters is not the actual E-field in space, but can be considered to be the *equivalent/normalized* E-field. It has been shown that the statistical behavior of the received voltage and the electric field are the same [11]. The gain of antenna 1 in the measured frequency range is around 10 dBi, thus a significant angular resolution can be obtained. Obviously, rotating an omnidirectional (axially symmetric) antenna is meaningless.

The measured *S*-parameters include an unstirred part $\tilde{S}_{us}$ and a stirred part $\tilde{S}_s$ [7]

$$\tilde{S} = \tilde{S}_{us} + \tilde{S}_s = \langle\tilde{S}\rangle + \tilde{S}_s\,, \tag{2}$$

where $\langle\cdot\rangle$ means the ensemble average using any stirring method (e.g. mechanical stir, frequency stir, source stir, *etc*.). Applying the IFFT to both sides of (2)

$$IFFT\left(\tilde{S}\right) = IFFT\left(\langle\tilde{S}\rangle\right) + IFFT\left(\tilde{S}_s\right), \tag{3}$$

where $IFFT\left(\tilde{S}\right)$ is the total time domain response and $IFFT\left(\langle\tilde{S}\rangle\right)$ is the unstirred part in the time domain. For an ideal/well-stirred reverberation chamber, $\langle\tilde{S}\rangle$ is the free-space *S*-parameter and $\langle\tilde{S}\rangle = \tilde{S}_{FreeSpace}$ [30]. When the RC is not ideal (stirrer efficiency is not 100%), the unstirred part $\langle\tilde{S}\rangle$ does not only include the free-space response, but also include the contribution of equivalent TSCS of stirrers (the moving objects in the RC). Only when the stirrer efficiency is high, is considering $\langle\tilde{S}\rangle$ as just the unstirred part of the free-space response a good approximation.

A. Statistical Behavior in the Time Domain

If we consider the statistical behavior of the impulse response in the time domain, the E-field can be regarded as a non-stationary stochastic process. For a specific time, because the incident waves are superimposed randomly, and applying the Lindberg central limit theorem [31], the rectangular E-field follows a normal distribution at each specific time. If the early time response and the unstirred part are ignored, the probability density function (PDF) can be expressed as

$$PDF[E(t)] = PDF[E_x(t)] = PDF[E_y(t)] = PDF[E_z(t)] = e^{-\frac{x^2}{2\sigma^2}}/(\sigma\sqrt{2\pi}) \quad (4)$$

with a mean value $\langle E(t)\rangle = 0$, and a time dependent standard deviation σ. An expression for $\sigma(t)$ can be found through the power decay $P(t)$ ($P(t) \propto E(t)^2$) which can be expressed

$$\langle P(t)\rangle = P_0 e^{-t\,\tau_{RC}^{-1}}, \quad (5)$$

where τ_{RC} is the decay constant of the RC, P_0 is a constant which determines the initial power. From (4), the PDF of $E(t)^2$ is found to follow the chi-square distribution with one degree of freedom

$$PDF[E(t)^2] \sim \chi_1^2 = e^{-\frac{x^2}{2\sigma^2}}/(\sigma\sqrt{2\pi x}) \quad (6)$$

and the mean value can be obtained as

$$\langle E(t)^2\rangle = \sigma^2. \quad (7)$$

If we compare (5) and (7), the time dependent σ can be obtained as

$$\sigma(t) = \sqrt{P_0 e^{-t\tau_{RC}^{-1}}}. \quad (8)$$

Thus the late time statistical behavior of the impulse response of the E-field is now well characterized. As can be seen later, it takes time for $\langle E(t)\rangle$ to decay and the decay speed is determined by the equivalent TSCS of the stirrers (i.e. how well the RC is stirred). Note that τ_{RC} is frequency dependent and can be considered as the average value in the spectrum range of the excitation impulse.

B. Stirrer Efficiency

The stirrer can be considered as an object under test [32], and the TSCS has been used to characterize the stirrer performance in simulations [33, 34]. It should be noted that, in the TSCS measurement, the object under test is required to be moved freely in space. However, in practice, the stirrers are rotating around fixed axes (cannot be moved freely), thus the measured TSCS is actually the *equivalent* TSCS. We denote the equivalent (measured) TSCS as $\widetilde{TSCS}$ and the $\widehat{TSCS}$ of stirrers can be obtained from $\langle E(t)^2\rangle$ and $\langle E(t)\rangle^2$ [32-34]

$$\langle E(t)^2\rangle = P_0 e^{-t\tau_{RC}^{-1}}, \quad (9)$$

$$\langle E(t)\rangle^2 = P_0 e^{-t(\tau_{RC}^{-1}+\tau_s^{-1})}. \quad (10)$$

A least-square fit can be applied to extract the chamber decay time τ_{RC} and the scattering damping time τ_s [32], and $\widehat{TSCS}$ of stirrers can be obtained as [32]

$$\widehat{TSCS} = \frac{V}{\tau_s c_0}, \quad (11)$$

where V is the volume of the RC, c_0 is the speed of light. If we check (9) - (11) carefully, it can be found that the contribution of τ_s is not sensitive to the load of the chamber, because the load of the chamber has been included in τ_{RC}. The contribution of τ_s can be extracted from

$$\frac{\langle E(t)\rangle^2}{\langle E(t)^2\rangle} = e^{-t\tau_s^{-1}}. \quad (12)$$

If we check (3), it can be found that, τ_s and $\widehat{TSCS}$ actually describes how fast the unstirred part decays compared with the total signal strength (power delay profile - PDP). If we define the *stirrer efficiency* as the residual of the ratio in (12) caused by the scattering damping time τ_s, we have

$$\eta_s = 1 - e^{-t_0\tau_s^{-1}}, \quad (13)$$

where t_0 is a typical/reference time (similar to the concept of typical physical dimension in [27, 35]). The stirrer efficiency is in the range 0% to 100%. It can be seen that when a very small stirrer is used, the stirrer efficiency is small, as there is no significant difference between (9) and (10), $\tau_{RC}^{-1} \approx (\tau_{RC}^{-1} + \tau_s^{-1})$, $\tau_s \to +\infty$, $\eta_s \to 0\%$. When the RC is well-stirred, $\langle E(t)\rangle^2$ decays to zero very fast and $\tau_{RC}^{-1} + \tau_s^{-1} \to +\infty$, $\tau_s \to 0$, $\eta_s \to 100\%$. In this paper we choose $t_0 = 12\sqrt[3]{V}/c_0$ which means the wave is allowed to interact with the walls of the RC at least twice, more discussions on t_0 are given in Appendix A. Then η_s in (13) becomes

$$\eta_s = 1 - e^{-12\sqrt[3]{V}/(c_0\tau_s)}. \quad (14)$$

(13) can also be written in the TSCS form using (11)

$$\eta_s = 1 - e^{-12\widehat{TSCS}/V^{2/3}}. \quad (15)$$

It is only related to the ratio between the equivalent TSCS of the stirrers and the surface area of the RC.

The definition in (13) confirms that τ_s is only related to $\widehat{TSCS}$ of stirrers which is not sensitive to the load and the antenna positions in the RC.

C. Time-Gating Technique

In the frequency domain, it is well-known that the chamber transfer function T can be corrected by removing the unstirred part of *S*-parameters [7]

$$T_{CFD} = \langle|S_{21} - \langle S_{21}\rangle|^2\rangle, \quad (16)$$

where T_{CFD} denotes the chamber transfer function is corrected in the frequency domain. Correspondingly, in the time domain, if we analyze (9) and (10), because of τ_s, $(\tau_{RC}^{-1} + \tau_s^{-1}) > \tau_{RC}^{-1}$, the unstirred part $\langle E(t)\rangle^2$ decays faster than $\langle E(t)^2\rangle$. This is

easy to understand, as the longer the wave travels, the more times it interacts with the stirrers. Filtering the signals in the time domain can also correct the unstirred part

$$T_{CTD} = \langle \left| FFT\{TG[IFFT(\tilde{S}_{21})]\} \right|^2 \rangle, \qquad (17)$$

where $\tilde{S}_{21}$ represents the filtered measured S21 between two antennas, TG means the time-gating operation which extracts the time domain signal through a chosen time window, FFT denotes the fast Fourier transform, T_{CTD} is the chamber transfer function corrected in the time domain. The philosophy is similar to what is done in the reflectivity measurement of radio absorbing material [36]: to measure the *S*-parameter in the frequency domain and transform the result into the time domain, then apply the time domain truncation to select the wanted signals; and finally, to transform the selected signals back to the frequency domain.

III. Measurement Results

We first rotate antenna 1 was rotated first but keep the stirrer position fixed, so there is no variable n in (1). The top view of the measurement setup inside the chamber is shown in Fig. 2(a), and typical filtered *S*-parameters S_{21} and S_{11} are shown in Fig. 2(b). Then antenna 1 is rotated with 2 degrees/step, and the IFFT is applied to all filtered *S*-parameters using Matlab. The bistatic and monostatic impulse time domain responses are denoted as $E_{21}(t,\theta)^2 = \{IFFT[\tilde{S}_{21}(\theta,f)]\}^2$ and $E_{11}(t,\theta)^2 = \{IFFT[\tilde{S}_{11}(\theta,f)]\}^2$ respectively. The bistatic and monostatic B-scan power maps in the range of 0 to 50 ns are shown in Fig. 3. In Fig. 3(a), where the color shows the received power level in dB of antenna 1 as a function of time and angle, the angle is defined in Fig. 2(a). This figure can also be viewed as a polar plot (or a radargram) where antenna 1 is located right in the middle of the plot (thus time is 0) and rotated as angle θ from 0 to 360°. From Fig. 2(a) and Fig. 3(a) (where the power is transmitted from antenna 1 to antenna 2), we can see that the line-of-sight (LoS) component can be seen clearly arrived first ($\theta \approx 45°$, the distance is 3 m between antenna 1 and antenna 2, the travelling time is 10 ns), followed by signals from the image sources ($\theta \approx 150°$ and $\theta \approx 280°$) that are also significant; In Fig. 3(b) (where the power is transmitted and received by antenna 1), reflections from walls and corners are easily identified and we can observe multiple reflections at $\theta = 0°$ and $\theta = 180°$, they are marked in the figure, also the reflection from the corners ($\theta \approx 315°$and $\theta \approx 225°$). For a monostatic map, the time needs to be divided by 2 when calculating the distance. Note the reflected wave from $\theta = 90°$ is diffused because of the vertical stirrer. The concentric circles in the center are reflections from the antenna itself which is independent of the rotation angle of the platform. The bistatic and monostatic B-scan power maps in the range of 0 to 500 ns are given in Fig. 4. As expected, the field is diffused as it travels in the RC.

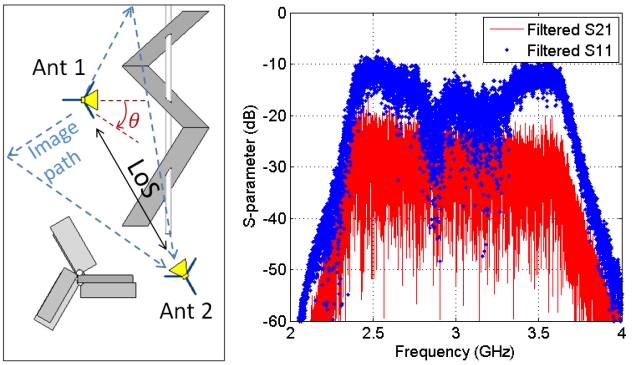

(a) (b)

Fig. 2. (a) Top view of B-scan measurement setup inside an RC and defined angle θ, (b) typical filtered *S*-parameters.

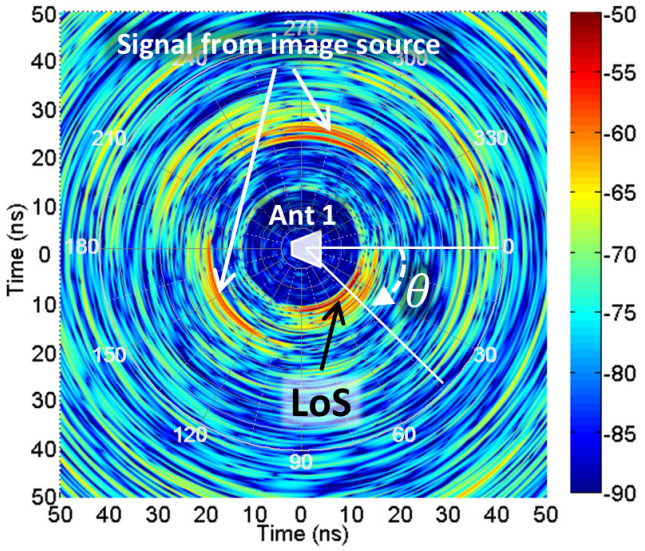

(a)

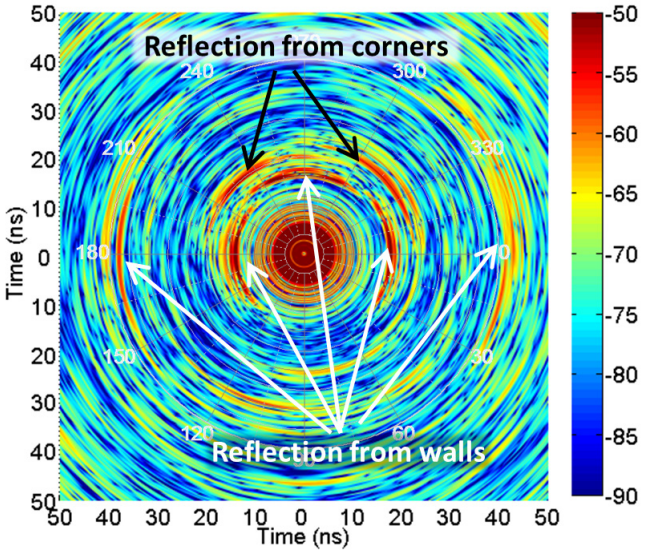

(b)

Fig. 3. B-scan in the range of 0 ~ 50 ns with stirrers fixed, the color represents the power in dB, (a) bistatic (from antenna 1 to antenna 2) map of $E_{21}(t,\theta)^2$, (b) monostatic (transmitted and received by antenna 1) map of,$E_{11}(t,\theta)^2$.

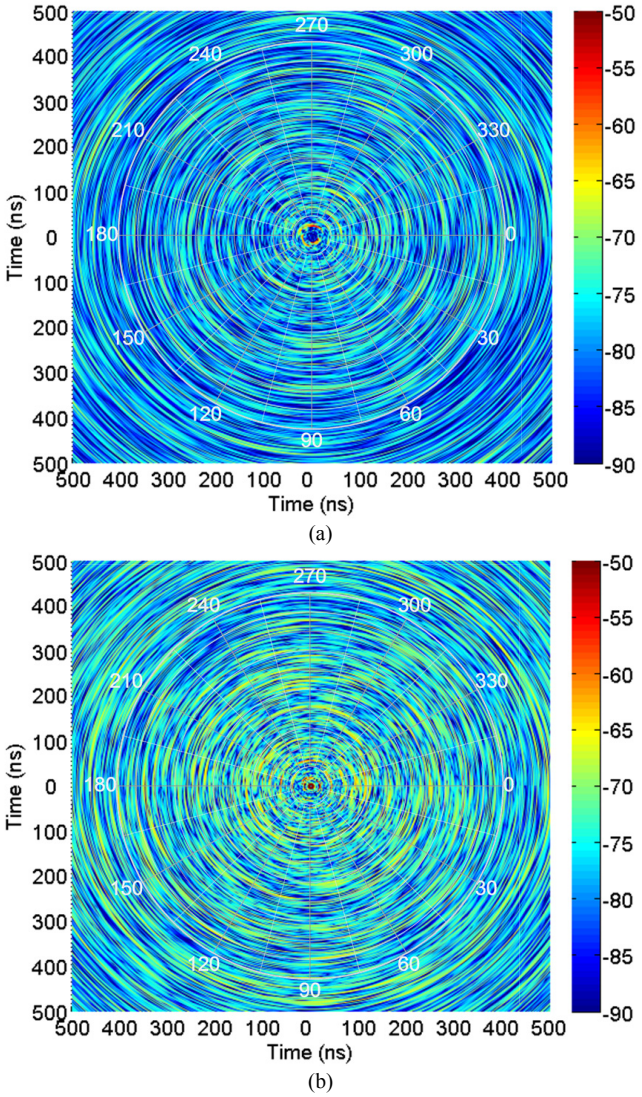

Fig. 4. B-scan in the range of 0 ~ 500 ns with stirrers fixed, (a) bistatic map $E_{21}(t,\theta)^2$ in dB unit, (b) monostatic map $E_{11}(t,\theta)^2$ in dB unit.

To investigate the angle dependency of the stirrer efficiency, 100 stirrer positions are used for each angle of antenna 1. The power delay profile (PDP) $\langle E_{21}(t,\theta)^2\rangle$ and $\langle E_{11}(t,\theta)^2\rangle$ are shown in Fig. 5, while the unstirred part $\langle E_{21}(t,\theta)\rangle^2$ and $\langle E_{11}(t,\theta)\rangle^2$ are shown in Fig. 6. As expected, (10) decays faster than (9), and the early time response from the walls cannot be cancelled, since the waves have not fully interacted with the stirrers yet. $\langle E_{21}(t)^2\rangle$ and $\langle E_{21}(t)\rangle^2$ for a fixed θ angle are shown in Fig. 7(a). It can be seen from Fig. 7(a) that, because the value of $(\tau_{RC}^{-1}+\tau_s^{-1})$ in (10) is not infinite, η_s is not 100%, $IFFT(\langle\tilde{S}\rangle) \neq IFFT(\tilde{S}_{FreeSpace})$. This explains the difference between the S-parameter measurement in the anechoic chamber and reverberation chamber [30]. The difference between $\langle\tilde{S}\rangle$ and $\tilde{S}_{FreeSpace}$ is due to the unstirred part which can be observed in the time domain, it does not only include the free-space response but also includes the contribution of $\overline{TSCS}$ (decay exponentially). In practice, if η_s is high, the difference between $\langle\tilde{S}\rangle$ and $\tilde{S}_{FreeSpace}$ is small, and $\tilde{S}_{FreeSpace}$ can still be measured in the RC.

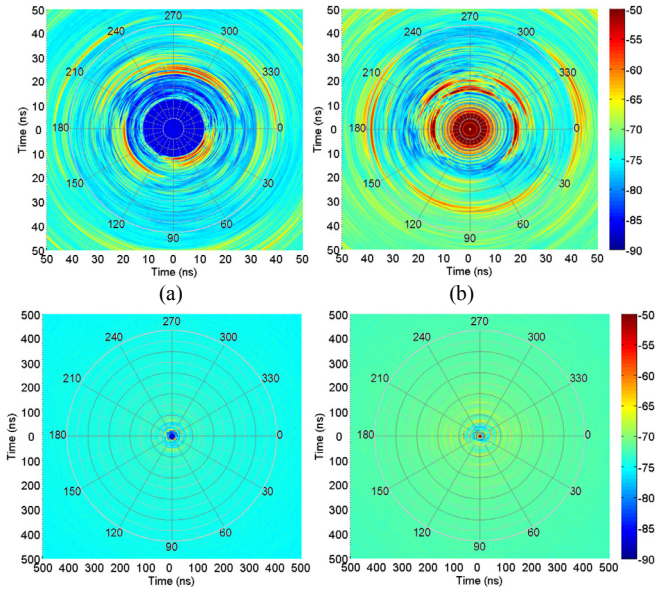

Fig. 5. PDP plot in dB unit, (a) $\langle E_{21}(t,\theta)^2\rangle$ in the range of 0 to 50 ns, (b) $\langle E_{11}(t,\theta)^2\rangle$ in the range of 0 to 50 ns, (c) $\langle E_{21}(t,\theta)^2\rangle$ in the range of 0 to 500 ns, (d) $\langle E_{11}(t,\theta)^2\rangle$ in the range of 0 to 500 ns.

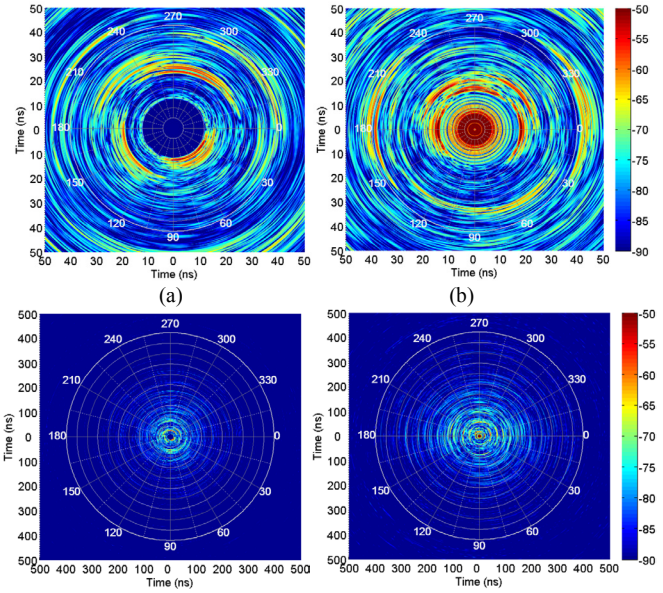

Fig. 6. Unstirred time-domain response in dB unit, (a) $\langle E_{21}(t,\theta)\rangle^2$ in the range of 0 to 50 ns, (b) $\langle E_{11}(t,\theta)\rangle^2$ in the range of 0 to 50 ns, (c) $\langle E_{21}(t,\theta)\rangle^2$in the range of 0 to 500 ns, (d) $\langle E_{11}(t,\theta)\rangle^2$ in the range of 0 to 500 ns.

The least-square fit is applied to extract τ_s in (10) [34]. As shown in Fig. 7(a), the slopes of $\langle E_{21}(t)^2\rangle$ and $\langle E_{21}(t)\rangle^2$ are k_1 and k_2, respectively. From (9) and (10), we have

$$\tau_{RC}^{-1} = -k_1 ln10/10\ , \tag{18}$$

$$\tau_{RC}^{-1}+\tau_s^{-1} = -k_2 ln10/10\ . \tag{19}$$

τ_s can be obtained as

$$\tau_s = \frac{10}{(k_1 - k_2) ln10} \tag{20}$$

or directly from the least-square fit using the ratio between $\langle E_{21}(t)\rangle^2$ and $\langle E_{21}(t)^2\rangle$ in (12). In Fig. 7(b), $E_{21}(t)$ and $\langle E_{21}(t)\rangle$ are also shown with time in log scale and magnitude in linear scale. As can be seen, at the beginning, the time domain response is dominated by the free-space response (first arrived waves), because of the contribution of $\widetilde{TSCS}$, $\langle E_{21}(t)\rangle$ decays faster than $E_{21}(t)$ in a few hundred nanoseconds, the decay speed is determined by τ_s in (20). For an ideal RC we have $IFFT(\langle \tilde{S} \rangle) = IFFT(\tilde{S}_{FreeSpace})$ which means $\langle E_{21}(t)\rangle$ decays so fast that $\tau_s \to 0$.

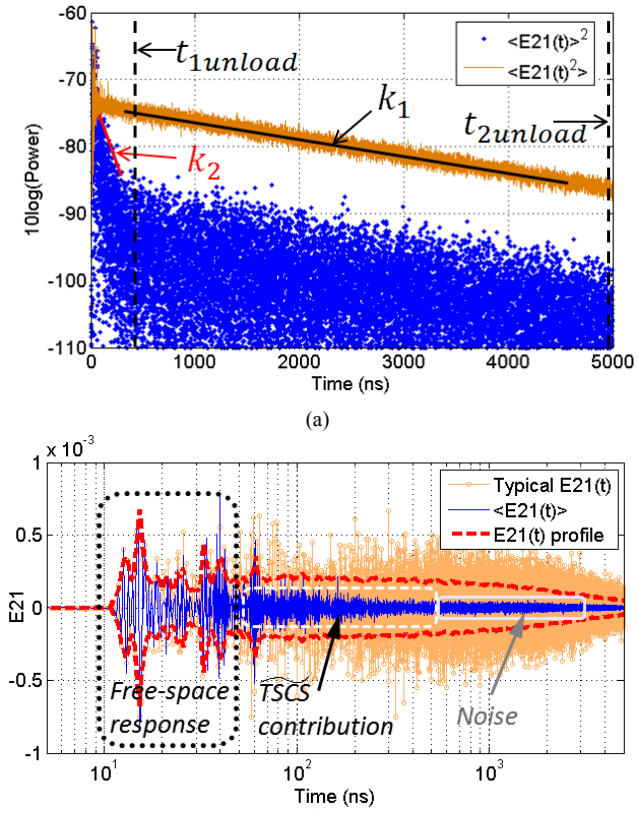

Fig. 7. (a) Typical $\langle E_{21}(t)^2\rangle$ and $\langle E_{21}(t)\rangle^2$ at a specific θ angle in dB scale, (b) typical $E_{21}(t)$, $\langle E_{21}(t)\rangle$ and E_{21} profile (square root of the PDP) plot in linear scale, dominated response in different time range are also marked.

It is expected that the load in the RC will not change the defined stirrer efficiency in this paper. In order to check the load effect on the stirrer efficiency, the whole measurement was repeated with the RC loaded with radio absorbing materials (AEP-X-CR from Microwave Vision Group). Loaded and unloaded τ_{RC}, η_s with different θ (antenna directions) are shown in Fig. 8. Obviously, τ_{RC} is not sensitive to antenna positions, we have $\tau_{RCload} = 993\, ns$, $\tau_{RCunload} = 1726\, ns$. Although τ_{RC} are different, we still have the same η_s, and η_s remains insensitive to the rotation angles (95.8 ± 2 %) as expected. As discussed previously, η_s depends on the equivalent TSCS of stirrers.

The unstirred part of the chamber transfer function is normally corrected in the frequency domain (16). Next we investigate the corrected chamber transfer function in the time domain (17). Suppose the time gate starts from t_1 and ends at t_2, for the loaded and unloaded RC, the power range must be the same, which means that we have the same initial and dissipated powers for the loaded and unloaded RC during the time gate (energy conservation). Otherwise, T_{CTD} in different scenarios cannot be compared because of different power dissipation. If the chamber buildup time is ignored [29], we have $P_0 e^{-t_{1unload}\tau_{RCunload}^{-1}} = P_0 e^{-t_{1load}\tau_{RCload}^{-1}}$, thus

$$t_{1unload}\tau_{RCunload}^{-1} = t_{1load}\tau_{RCload}^{-1}, \tag{21}$$

$$t_{2unload}\tau_{RCunload}^{-1} = t_{2load}\tau_{RCload}^{-1}. \tag{22}$$

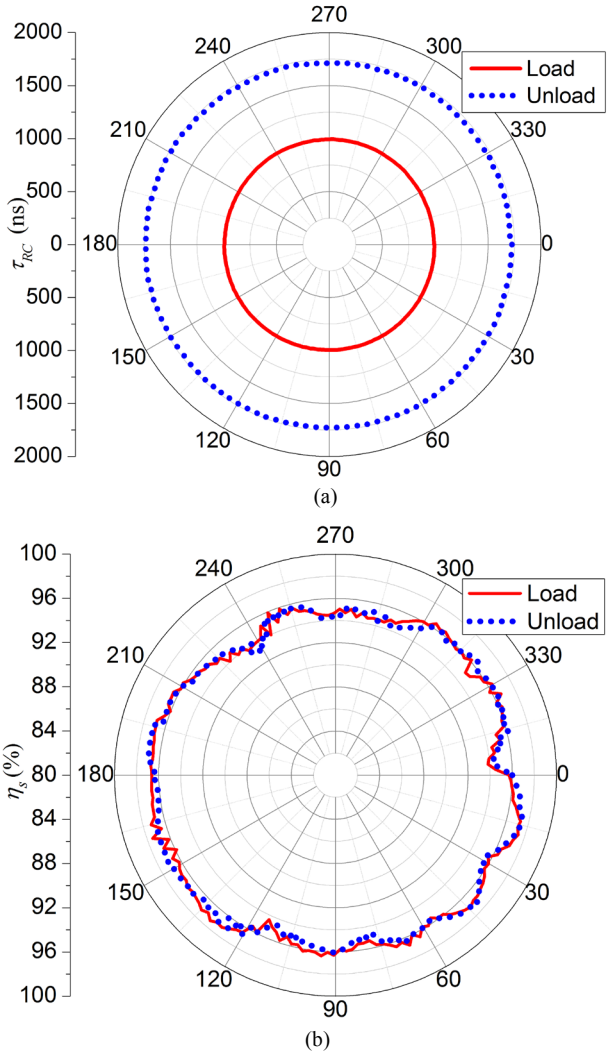

Fig. 8. Loaded and unloaded τ_{RC} (a) and η_s (b) with different θ (antenna directions).

As can be seen in Fig. 7(a), after 500 ns, the unstirred part is quite small (10 dB smaller than the PDP/total signal), we use $t_{1unload} = 500\, ns$, $t_{2unload} = 5000\, ns$ for the unloaded RC and $t_{1load} = 288\, ns$, $t_{2load} = 2876\, ns$ for the loaded RC respectively.

The results are shown in Fig. 9, a frequency stir with nearest 100 frequency points is used. The uncorrected chamber transfer

function $\langle|S_{21}|^2\rangle$ is given first in Fig. 9(a), because of the unstirred part, it shows angle dependency. The angle dependency of K-factor in dB is also shown in Fig. 9(b). At each θ angle, the K-factor is calculated using the unbiased estimator [14]

$$K = \frac{N-2}{N-1}\left\langle \frac{|\langle S_{21}\rangle|^2}{|S_{21}-\langle S_{21}\rangle|^2} \right\rangle - \frac{1}{N}, \qquad (23)$$

where $N = 100$ with a frequency stir with 100 nearest frequencies. The corrected chamber transfer function using (16) and (17) are given in Fig. 9(c) and (d). As expected, no angle dependency is observed which means both methods can remove the unstirred component. A comparison between T_{CFD} and T_{CTD} is given in Fig. 10, because part of the time domain signal is filtered by using time gating, this results in $T_{CTD} < T_{CFD}$. It is not an issue, because normally we are interested in the relative T rather than the absolute T, and it can be seen in Fig. 10(b) that there is a very good agreement between $T_{CFDload} - T_{CFDunload}$ and $T_{CTDload} - T_{CTDunload}$. The small deviation (< 0.2 dB) could be due to the ignorance of the different chamber buildup time in (21) and (22), which leads to slightly different total energy for the loaded and unloaded RC in the time gate.

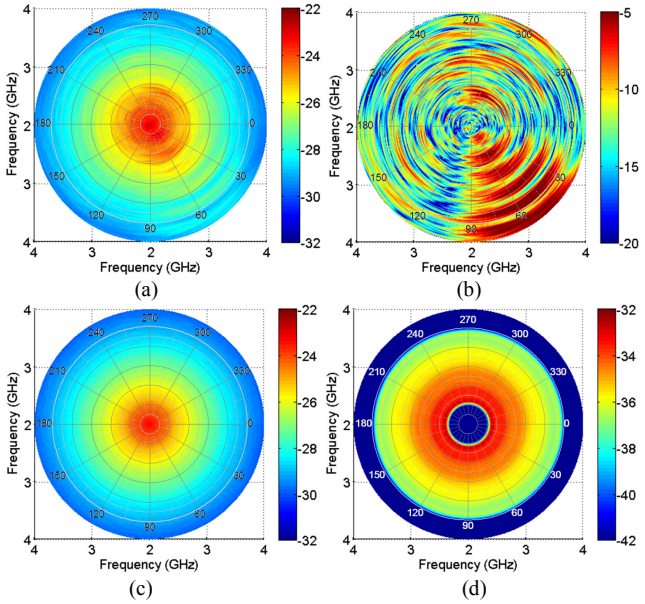

Fig. 9. (a) Uncorrected chamber transfer function $\langle|S_{21}|^2\rangle$, (b) K-factor, (c) T_{CFD}, (d) T_{CTD}, the RC is unloaded.

It is interesting to note that, even though the two antennas are positioned in LoS, the K-factor can still be very small at some specific frequencies (Fig. 11). Remember the unstirred part is not only from the LoS, it can be also from the walls (specular reflection [2]) and other structures (also the contribution of $\overline{TSCS}$), when the waves from these objects cancel each other at some frequencies, a small K-factor is observed.

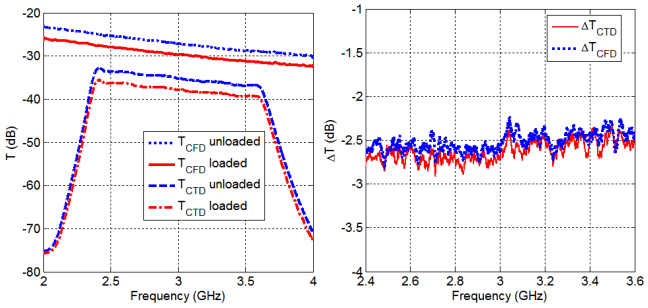

Fig. 10. (a) Corrected chamber transfer functions, (b) difference between loaded and unloaded T, $\Delta T_{CFD} = T_{CFDload} - T_{CFDunload}$, $\Delta T_{CTD} = T_{CTDload} - T_{CTDunload}$.

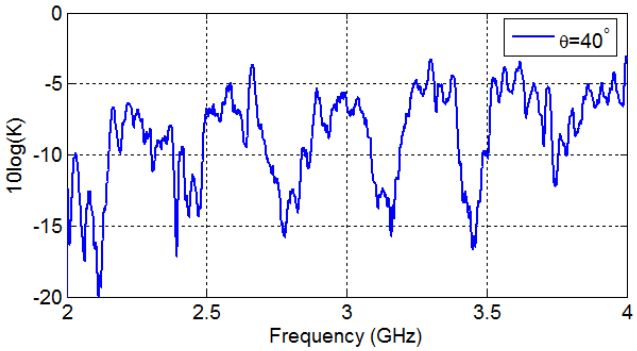

Fig. 11. K-factor in dB at $\theta = 40°$, the RC is unloaded.

We have measured the stirrer efficiency in a bandwidth of 1.2 GHz (2.4 GHz ~ 3.6 GHz) with different angle of antenna 1 (Fig. 8(b)). Measurement scenarios are summarized in Table I. Since τ_{RC} and τ_s are frequency dependent, η_s is also frequency dependent. If we use a smaller bandwidth (200 MHz) and sweep the center frequency, a frequency dependency of stirrer efficiency can be observed (like the extraction of τ_{RC} in [7]). Further measurement scenarios are implemented and given in Table II, we rotate only the horizontal stirrer, only the vertical stirrer and both stirrers, respectively. Because of the limitation of the maximum sample number of the VNA, the frequency range of 0.2 GHz ~ 4.1 GHz is divided into three bands with 10001 sample points in each band, thus we have total 30003 sample points. The measurement time for one antenna position with 360 stirrer positions in one band is 8 hours. Finally, we remove half of the vertical stirrer (Fig. 12(a)) and repeat the measurement with 10 random antenna positions to check if there is any relation between the K-factor and η_s. One of them is the extreme scenario which is in LoS (Fig. 12(b)).

TABLE I
MEASUREMENT SCENARIOS

Scenario	Stirrer Position No.	Platform Position No.	Load /Unload	Measurement Time
1	1	180	Unload	4 hours
2	100	180	Unload	402 hours
3	100	180	Load	402 hours

TABLE II
FURTHER MEASUREMENT SCENARIOS

Scenario	Stirrer Position No.	Load /Unload	Antenna Position No.	Frequency Range
Only H	360	Load	1	0.2 GHz ~4.1 GHz (30003 points)
Only V	360	Load	1	0.2 GHz ~4.1 GHz (30003 points)
H & V	360	Load	1	0.2 GHz ~4.1 GHz (30003 points)
Small V*	360	Load	10	1.9 GHz ~4.1 GHz (10001 points)

* Small V means half of the vertical stirrer is removed shown in Fig. 12.

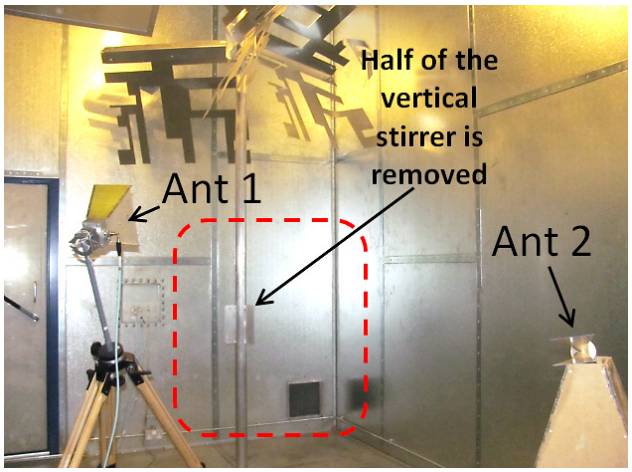

(a)

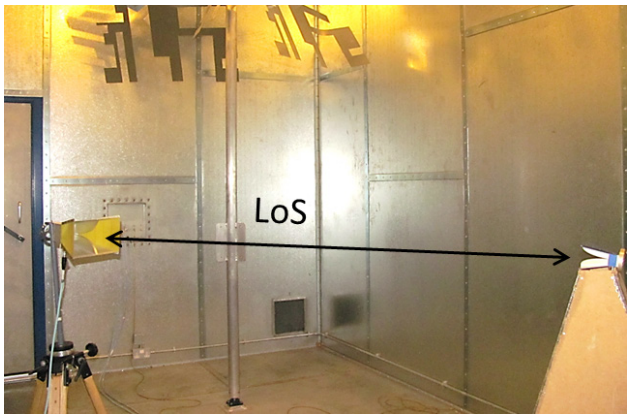

(b)

Fig. 12. Measurement with half of the vertical stirrer, (a) a typical random antenna position, (b) LoS setup.

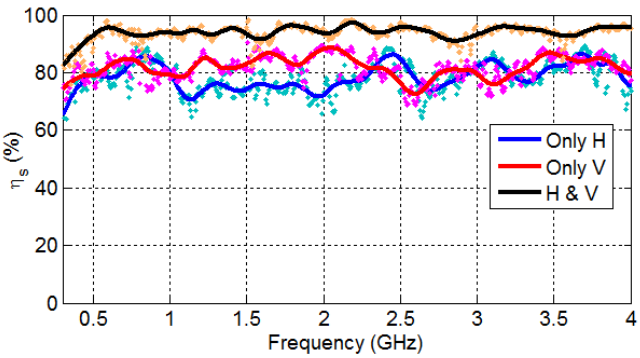

Fig. 13. Stirrer efficiency with different stirrer rotation, light dot is the measured result; solid line is the smoothed result.

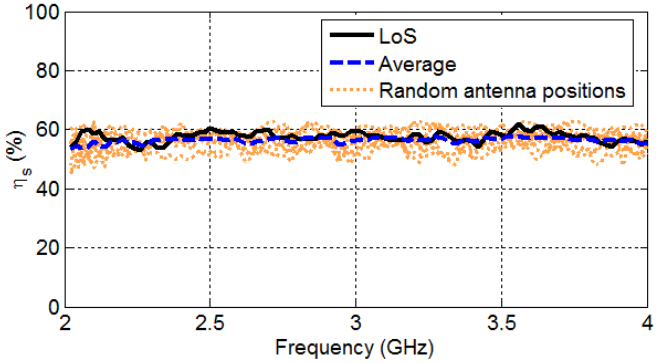

Fig. 14. Stirrer efficiency with half of the vertical stirrer (10 random antenna positions are used with 1 LoS).

The results are given in Fig. 13 and Fig. 14, and *K*-factors with random antenna positions are given in Fig. 15. As expected, when both stirrers are used, we have the highest stirrer efficiency (which demonstrates the importance of using both) and a smaller stirrer gives small stirrer efficiency. Although the *K*-factor has a large variation (~15 dB), they do not affect the stirrer efficiency. The LoS component only affects the initial response in a few nanoseconds, but the decay speed in a few hundred nanoseconds (Fig. 16) is determined by the equivalent TSCS of the stirrers and is not sensitive to the antenna position.

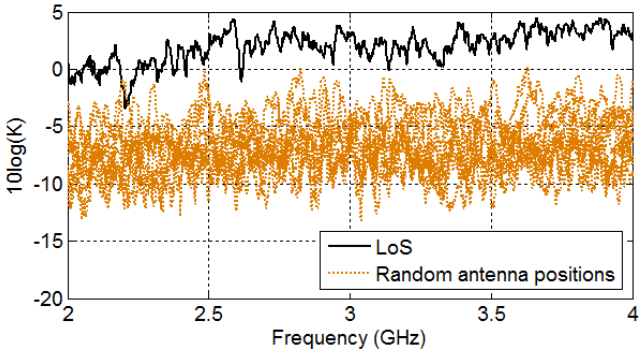

Fig. 15. *K*-factor in dB with half of the vertical stirrer (10 random antenna positions are used with 1 LoS).

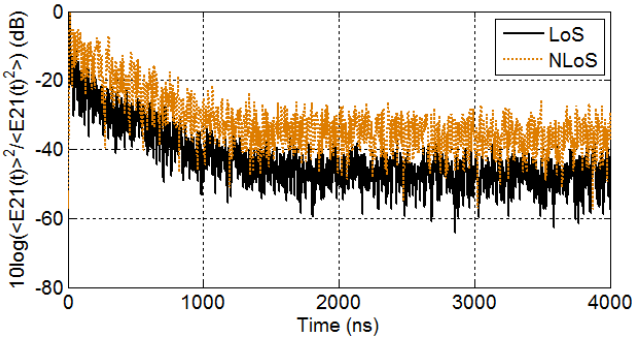

Fig. 16. $\langle E(t)\rangle^2/\langle E(t)^2\rangle$ in dB with half of the vertical stirrer, a comparison between LoS and non-line-of-sight (NLoS).

If we check the mean value of η_s, it can be found that the mean value of η_s of the half vertical stirrer is around 55%, this corresponds to the $\overline{TSCS}$ of $0.0665V^{2/3}$ in (15). Because the

TSCS can be superimposed under the dilute approximation [32, 37], if a whole vertical stirrer is used, the $\widetilde{TSCS}$ is roughly $2 \times 0.0665V^{2/3}$, this corresponds to a stirrer efficiency of 80% which agrees well with the results in Fig. 13. We have also compared stirrer efficiency between the horizontal and vertical stirrers in Fig. 13. The $\widetilde{TSCS}$ of the two stirrers is around $2 \times 2 \times 0.0665V^{2/3}$, this corresponds to the stirrer efficiency of 96% which agrees well with the H & V results in Fig. 13. Thus from (15) we have

$$\eta_{stot} = 1 - \prod_{i=1}^{N}(1 - \eta_{si}), \tag{24}$$

where η_{si} is the stirrer efficiency with only *i*-th stirrer, η_{stot} is the stirrer efficiency when all *N* stirrers are moving together.

An important question is: how to increase the stirrer efficiency? Obviously a big stirrer or many stirrers working together is better. From (24), this phenomenon is quantified, we can have a big η_{s1} with $N = 1$ (the trade-off is a reduction of the test volume) or small η_{si} with a big N. Source stir is also a method to improve the performance of the RC [38, 39]. Actually, if we consider the moving antenna as the stationary coordinate frame, rotating the antenna is actually rotating the whole RC, which obviously has a large $\widetilde{TSCS}$. We have also tried to aim the antenna at the stirrer (in 10 random antenna positions in Fig. 12), because there are always leaky waves (from side lobes, back lobes, scattering from rotation axis and stationary object) which do not fully interact with the moving stirrer, otherwise the stirrer and the antenna can be considered to be an integrated big antenna and the moving of the stirrer becomes the moving of the source (source stir). To verify this, we use the data from scenario 1 in Table I to calculate the stirrer efficiency (keep the stirrers steady and rotate the antenna), nearly 100% stirrer efficiency is obtained in the frequency range of 2.4 GHz ~ 3.6 GHz. The ratio between $\langle E(t)\rangle^2$ and $\langle E(t)^2\rangle$ is shown in Fig. 17, it drops down to the noise level in 100 ns which demonstrates that the source stirred method could produce a high efficiency RC.

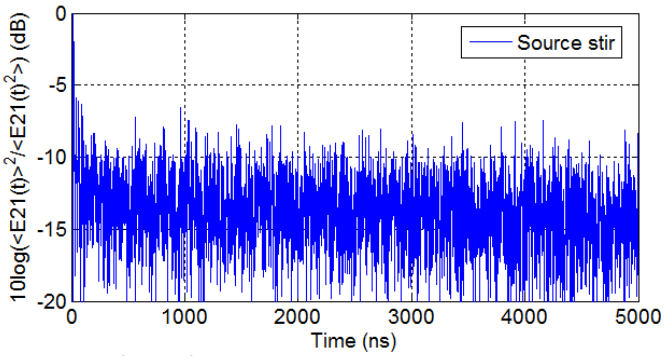

Fig. 17. $\langle E(t)\rangle^2/\langle E(t)^2\rangle$ in dB using the source stir method.

IV. Discussion and Conclusions

In this paper, an in-depth study of very fine B-scan measurements has been performed. Based on the B-scan results, this paper has been focused on three aspects: the statistical behavior of the E-field in the time domain, stirrer efficiency quantification, and a time-gating technique. Since we aim to present a complete B-scan image which is very time consuming to yield, if only the stirrer efficiency needs to be measured, measurements at a few antenna positions are enough.

It has been shown in this paper that the late-time E-field can be regarded as a non-stationary stochastic process with Gaussian distribution; the standard deviation is time dependent and related to the chamber decay time (8).

The stirrer efficiency proposed in this paper is only related to the equivalent TSCS of stirrers (the moving object in the RC) and the volume of the RC, which is not sensitive to the antenna position and the load of the RC, thus it provides a general way to compare the performance of different RCs or one chamber with different stirrers. The proposed definition is intuitive and can be understood from another point of view: a small stirrer means the wave needs to travel a relatively long time and interact with stirrers more times to become random enough (a slow $\langle E(t)\rangle^2$ decay), while a big stirrer means the wave can become random quickly (a fast $\langle E(t)\rangle^2$ decay). Because $\widetilde{TSCS}$ can be superimposed, which means the stirrer efficiency is predictable, this is important for the RC design, the designer can evaluate how large a stirrer needs to be (or how many stirrers are needed) based on the existing design using (24).

A time-gating technique in the RC has been proposed, which provides an alternative method to correct the unstirred part in the time domain. It should be noted that when using this time-gating technique to compare the transfer functions in the unloaded and loaded RCs, the start time and the end time of the time gate are different. The time-gating technique can be used to improve the stirrer efficiency: by filtering the early time response, the unstirred part of S-parameters can be filtered. For antenna measurements the time domain response can easily be truncated, for other measurements if the time domain response cannot be easily separated (radiated susceptibility or radiated emission measurement), physically high stirrer efficiency is still required.

The difference between the stirrer efficiency defined in this paper and the field uniformity (FU) should be noted. The FU is determined by the measured average E-field in the frequency domain [19] which includes both the unstirred part and stirred part. Stirrer efficiency describes how fast the unstirred part decays compared with the total response or how fast the total signal is dominated by the stirred part. It also describes the difference between $\langle \tilde{S} \rangle$ and $\tilde{S}_{FreeSpace}$, as discussed before, $\langle \tilde{S} \rangle$ does not only include the free-space response (in a few nanoseconds), but also include the contribution of $\widetilde{TSCS}$ of moving objects (in a few hundred nanoseconds), we need $\langle E(t)\rangle^2$ to decay very fast to ensure that the unstirred part is dominated by the free space response, that is when $\eta_s \rightarrow 100\%$, $\langle \tilde{S} \rangle \rightarrow \tilde{S}_{FreeSpace}$.

To have a good RC, the stirred part needs to be as uniform as possible and the unstirred part needs to be as small as possible. The use of diffusers [40, 41] on the specular reflection wall

actually diffuses the unstirred part to improve the field uniformity, but the stationary diffusers cannot change the $\widetilde{TSCS}$ of the stirrers thus cannot change the stirrer efficiency (the decay speed of $\langle E(t)\rangle^2$). However, if only the field uniformity is used as the standard it is already a good RC, unless for some special applications (e.g. to measure the free space *S*-parameters in an RC) we need $IFFT(\langle\tilde{S}\rangle) = IFFT(\tilde{S}_{FreeSpace})$ ($\langle\tilde{S}\rangle$=$\tilde{S}_{FreeSpace}$).

High stirrer efficiency does not necessarily mean a good FU (when a high directivity antenna direct to the test region) and a good FU does not necessarily mean high stirrer efficiency (both stirred part and unstirred part are uniform but the unstirred part decays slowly in time domain). Normally, if the stirrer efficiency is high and the *K*-factor is small, the field in the test region is dominated by the stirred part, if the stirred part is uniform, a good FU is obtained (except some special cases the stirred part can also be non-uniform [42]). It should also be noted that in this paper, the RC works in an overmoded condition (the baseline of an RC), otherwise the PDP no longer decays exponentially [43] and the definition of τ_{RC} and τ_s are no longer valid.

APPENDIX A
THE CHOICE OF TYPICAL TIME

An appropriate typical/reference time t_0 need to be chosen to determine η_s. Assume the shape of the RC is a cube, if the wave is allowed to interact with all the walls inside the RC at least twice (the wave follows the red dot line in Fig. 18), the travel time is $12\sqrt[3]{V}/c_0$.

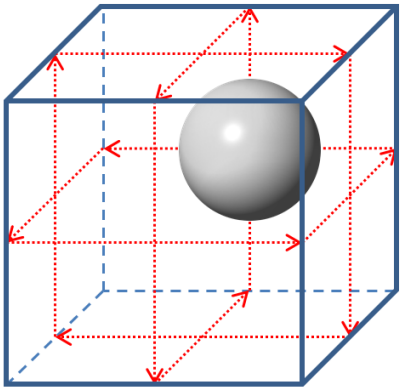

Fig. 18. An intuitive explanation of the wave interaction with the boundaries in a cubic RC, a sphere with radius $r = V^{1/3}/\sqrt{8\pi}$ is also shown.

As can be seen, when $\widetilde{TSCS} = V^{2/3}/4$ (a quarter of the surface area of a face in Fig. 18), $\eta_s = 1 - e^{-3} = 95.0\%$. This is a reasonable value to our knowledge, if we have such a large sphere with radius $r = V^{1/3}/\sqrt{8\pi}$ which can move freely in the RC, the stirrer efficiency should be high (the TSCS of the sphere is $2\pi r^2 = V^{2/3}/4$ when the electrical size is large [32]). Normally, the stirrers are rotating around fixed axes, the equivalent TSCS is smaller than the real TSCS of the stirrers.

It should be noted that, theoretically there are infinite ways to map $\widetilde{TSCS}/V^{2/3}$ to the range of 0% to 100%. If we use a variable α to control the allowed travel time and let $t_0 = \alpha\sqrt[3]{V}/c_0$, η_s with different α values are shown in Fig. 19. As can be seen, when α is small, high stirrer efficiency becomes hard to achieve, which means a very short time is allowed for the waves to travel to become random. In practice, we need an appropriate value to have an intuitive understanding and it is not reasonable to have a too small (high η_s can never be achieved) or too large α (always give a high η_s). In this paper, $\alpha = 12$ is recommended.

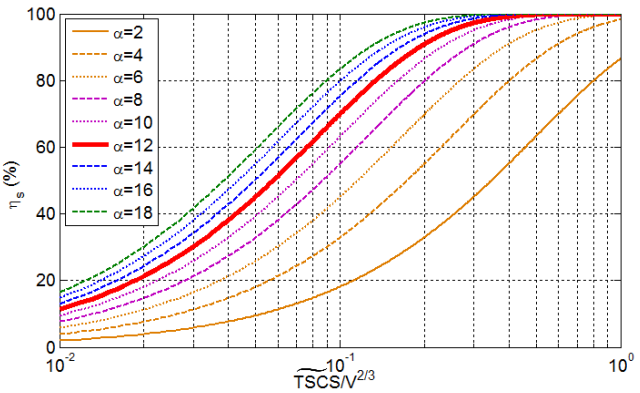

Fig. 19. η_s curves with different α values.

REFERENCES

[1] R. J. Pirkl and K. A. Remley, "Experimental evaluation of the statistical isotropy of a reverberation chamber's plane-wave spectrum," *IEEE Trans. EMC*, vol. 46, no. 3, pp. 498-509, Jun. 2014.

[2] R. J. Pirkl, J. M. Ladbury and K. A. Remley, "The reverberation chamber's unstirred field: A validation of the image theory interpretation," IEEE International Symposium on EMC, pp. 670-675, Long Beach, USA, Aug. 2011.

[3] A. Sorrentino, A. Gifuni, G. Ferrara and M. Migliaccio, "Mode-stirred reverberation chamber autocorrelation function: model, multifrequency measurements and applications," *IET Science, Measurement & Technology*, vol. 9, no. 5, pp. 547-554, 2015.

[4] A. Sorrentino, A. Gifuni, G. Ferrara and M. Migliaccio, "Mode-stirred reverberation chamber Doppler spectra: multi-frequency measurements and empirical model," *IET Microwave Antenna & Propagation*, vol. 8, no. 15, pp. 1356-1362, 2014.

[5] P. Corona, G. Ferrara and M. Migliaccio, "Polarimetric field characterization in reverberating chambers," *IEEE Trans. EMC*, vol. 46, no. 2, pp. 155-159, 2004.

[6] G. Gradoni, V. M. Primiani and F. Moglie, "Reverberation chamber as a statistical relaxation process: entropy analysis and fast time domain simulations," International Symposium on Electromagnetic Compatibility (EMC EUROPE), pp.1-6, Rome, Italy, Sept. 2012.

[7] C. L. Holloway, H. A. Shah, R. J. Pirkl, W. F. Young, D. A. Hill and J. Ladbury, "Reverberation chamber techniques for determining the radiation and total efficiency of antennas," *IEEE Trans. Antennas Propagat.*, vol. 60, no. 4, pp. 1758-1770, Apr. 2012.

[8] U. Calberg, P. –S., Kildal, A. Wolfgang, O. Sotoudeh and C. Orlenius, "Calculated and measured absorption cross sections of lossy objects in reverberation chamber," *IEEE Trans. EMC*, vol. 46, no. 2, pp. 146-154, May 2004.

[9] E. Genender, C. L. Holloway, K. A. Remley, J. M. Ladbury, G. Koepke and H. Garbe, "Simulating the multipath channel with a reverberation chamber: application to bit error rate measurements," *IEEE Trans. EMC*, vol. 52, no. 4, pp. 766-777, Nov. 2010.

[10] D. J. Daniels, *Ground Penetration Radar*, 2nd Ed, The IEE Press, 2004.

[11] D. A. Hill, *Electromagnetic Fields in Cavities: Deterministic and Statistical Theories*, Wiley-IEEE Press, 2009.

[12] D. A. Hill, "Uniqueness of plane wave integral representation for idealized fields in reverberation chambers," *IEEE Trans. EMC*, vol. 57, no. 3, pp. 584-586, June 2015.

[13] O. Lunden and M. Backstrom, "Stirrer efficiency in FOA reverberation chambers. Evaluation of correlation coefficients and chi-squared tests,"

IEEE International Symposium on EMC, pp. 11-16, Washington DC, USA, Aug. 2000.
[14] C. Lemoine, E. Amador and P. Besnier, "Mode-stirring efficiency of reverberation chambers based on Rician K-factor," *Electronic Letters*, vol. 47, no. 20, Sep. 2011.
[15] C. Lemonie, P. Besnier and M. Drissi, "Evaluation of frequency and mechanical stirring efficiency in a reverberation chamber," International Symposium on Electromagnetic Compatibility – EMC Europe, pp. 1-6, Hamburg, German, Sep. 2008,
[16] J. Clegg, A. C. Marvin, J. F. Dawson and S. J. Porter, "Optimization of stirrer designs in a reverberation chamber," *IEEE Trans. EMC*, vol. 47, no. 4, pp. 824-832, Nov. 2005.
[17] C. L. Holloway, D. A. Hill, J. M. Ladbury and G. Koepke, "Requirements for an effective reverberation chamber: unloaded or loaded," *IEEE Trans. EMC*, vol. 48, no. 1, pp. 187-194, Feb. 2006.
[18] C. L. Holloway, D. A. Hill, J. M. Ladbury, P. F. Wilson, G. Koepke and J. Coder, "On the use of reverberation chambers to simulate a Rician radio environment for the testing of wireless deveices," *IEEE Trans. Antennas Propagat.*, vol. 54, no. 11, pp. 3167-3177, Nov. 2006.
[19] Electromagnetic compatibility (EMC) – Part 4-21: Testing and measurement techniques – Reverberation chamber test methods, IEC 61000-4-21, Ed 2.0, 2011.
[20] F. Moglie and V. M. Primiani, "Analysis of the independent positions of reverberation chamber stirrers as a function of their operating conditions," *IEEE Trans. EMC*, vol. 53, no. 2, pp. 288-295, May 2011.
[21] S. Pfenning, H. G. Krauthauser, "A general method for determining the number of independent stirrer positions in reverberation chambers," IEEE International Symposium on Electromagnetic Compatibility, pp. 1-6., Rome, Italy, 2012.
[22] C. Lemonie, P. Besnier and M. Drissi, "Estimating the effective sample size to select independent measurements in a reverberation chamber," *IEEE Trans. EMC*, vol. 50, no. 2, pp. 227-236, May 2008.
[23] X. Chen, "Experimental investigation of the number of independent samples and the measurement uncertainty in a reverberation chamber," *IEEE Trans. Antennas Propagat.*, vol. 55, no. 5, pp. 816-824, Oct. 2013.
[24] V. Rajamani, C. F. Bunting and J. C. West, "Effects of loading on independent samples and uniformity of a reverberation chamber," IEEE International Symposium on Electromagnetic Compatibility, pp. 207-216., Denver, USA, 2013.
[25] G. Esposito, G. Gradoni, F. Moglie and V. M. Primiani, "Stirrer performance of reverberation chambers evaluated by time domain fidelity," IEEE International Symposium on Electromagnetic Compatibility, pp. 207-216., Denver, USA, 2013.
[26] W. T. C. Burger, C. L. Holloway and K. A. Remley, "Proximity and orientation influence on Q-factor with respect to large-form factor loads in a reverberation chamber," Poc. of the 2013 International Symposium on Electromagnetic Compatibility, pp. 369-374, Brugge, Belgium, Sep. 2013.
[27] E. Amador, C. Lemonie, P. Besnier and A. Laisné, "Reverberation chamber modeling based on image theory: Investigation in the pulse regime," *IEEE Trans. EMC,* vol. 52, no. 4, pp.778-789, Nov. 2010.
[28] S. M. H. A. Shah, "Wireless channel characterization of the reverberation chamber at NIST," M.S. thesis, Department of Signals and System, Chalmers University of Technology, Gothenburg, Sweden, 2011.
[29] C. L. Holloway, H. A. Shah, R. J. Pirkl, K. A. Remley, D. A. Hill and J. Ladbury, "Early time behavior in reverberation chambers and its effect on the relationships between coherence bandwidth, chamber decay time, RMS delay spread, and the chamber buildup time," *IEEE Trans. EMC,* vol. 54, no. 4, pp.717-725, Nov. 2012.
[30] P. –S. Kildal, C. Carlsson and J. Yang, "Measurement of free-space impedances of small antennas in reverberation chambers," *Microwave and Optical Technology Letters*, vol. 32, no. 2, pp. 112-115, Dec. 2001.
[31] R. V. Hogg and E. A. Tanis, *Probability and Statistical Interference*, 7th Ed, Pearson, 2005.
[32] G. Lerosey and J. de Rosny, "Scattering cross section measurement in reverberation chamber," *IEEE Trans. EMC,* vol. 52, no. 2, pp.280-284, May. 2007.
[33] S. Lallechere, I. E. Baba, P. Bonnet and F. Paladian, "Total scattering cross section improvements from electromagnetic reverberation chambers modelling and stochastic formalism," in Proceeding of the 5th European Conference on Antennas and Propagation (EUCAP), pp. 81-85, Rome, Italy, Apr. 2011.
[34] I. E. Baba, S. Lallechere, P. Bonnet, J. Benoit and F. Paladian, "Computing total scattering cross section from 3-D reverberation chambers time modelling," Asia-Pacific Symposium on Electromagnetic Compatibility (APEMC), Singapore, May 2012.
[35] E. Amador, C. Lemoine and P. Besnier, "An empirical statistical detection of non-ideal field distribution in a reverberation chamber confirmed by a simple numerical model based on image theory," *Ann. Telecommun.*, vol. 66, pp. 445-455, Aug. 2011.
[36] IEEE recommended practice for radio-frequency (RF) absorber evaluation in the range of 30 MHz to 5 GHz, IEEE Standard 1128-1998, Apr. 1998.
[37] A. Ishimaru, *Wave Propagation and Scattering in Random Media*, vol. 2, New York: Academic, 1978, ch. 14, pp. 253-294.
[38] Y. Huang and D. J. Edwards, "A novel reverberating chamber: source-stirred chamber," Proc. Of IEE 8th International Conference on Electromagnetic Compatibility, pp. 120-124, Edinburgh, UK, Sep. 1992.
[39] K. Rosengren, P. –S. Kildal, C. Carlsson and J. Carlsson, "Characterization of antennas for mobile and wireless terminals in reverberation chambers: improved accuracy by platform stirring," *Microwave and Optical Technology Letters*, vol. 39, no. 6, pp. 391-397, Sep. 2001.
[40] J. –C. Yun, J. –G. Rhee and S. –Y. Chung, "An improvement of field uniformity of reverberation chamber by the variance of diffuser volume ratio," Asia-Pacific Microwave Conference (APMC), vol. 3, pp. 1123-1126, Taipei, Dec. 2001.
[41] A. C. Marvin and E. Karadimou, "The use of wave diffusers to reduce the contribution of specular wall reflections to the unstirred energy in a reverberation chamber," IEEE International Symposium on Electromagnetic Compatibility, pp. 227-231, Denvor, USA, Aug. 2013.
[42] J. A. D. Toorn, K. A. Remley, C. L. Holloway, J. M. Ladbury and C. Wang, "Proximity-effect test for lossy wireless-device measurements in reverberation chambers," *IET Science, Measurement & Technology*, vol. 9, no. 5, pp. 540-546, 2015.
[43] C. R. Dunlap, "Reverberation chamber characterization using enhanced backscatter coefficient measurements," Ph.D. dissertation, Dept. of Electrical, Computer and Engineering, University of Colorado, Boulder, USA, 2013.